nature communications

Article

https://doi.org/10.1038/s41467-024-54801-1

Identification and structure-guided development of triazole urea-based selective antagonists of *Arabidopsis* karrikin signaling

Received: 8 July 2023

Accepted: 22 November 2024

Published online: 02 January 2025

Check for updates

Jianwen Wang[1,5], Ikuo Takahashi[1,5], Ko Kikuzato[1], Toshihiko Sakai[1], Zhangliang Zhu[1,2], Kai Jiang[1,4], Hidemitsu Nakamura[1], Takeshi Nakano[2], Masaru Tanokura[1], Takuya Miyakawa[1,2] ✉ & Tadao Asami[1,3] ✉

The smoke-derived butenolides, karrikins (KARs), regulate many aspects of plant growth and development. However, KARs and a plant hormone, strigolactones (SLs), have high resemblance in signal perception and transduction, making it hard to delineate KARs response due to the shortage of chemical-genetic tools. Here, we identify a triazole urea KK181N1 as an inhibitor of the KARs receptor KAI2. KK181N1 selectively depress the KAR-induced phenotypes in *Arabidopsis*. We further elucidate the antagonistic, KAI2 binding mechanism of KK181N1, showing that KK181N1 binds to the catalytic pockets of KAI2 in a non-covalent binding manner. Our experiments also demonstrate the binding affinity of triazole urea compounds are regulated by the structured water molecule networks. By fine-tuning this network, we successfully develop a more potent derivative of KK181N1. We anticipate that these chemicals will be applicable to the elucidation of KARs biology, especially for discriminating the molecular and physiological aspects of KARs and SL signaling.

Vegetation fire has long been necessary for reshaping the ecosystems in nature[1]. The produced smoke and ash are thought to be a primary source of the nutrients that allow plants to thrive[2]. The germination of dormant seeds produced by fire-adapted plant species is stimulated by specific chemicals in the smoke-laden water after a wildfire[3]. One of the potent germination-stimulating compounds to be isolated and identified from such smoke was 3-methyl-2*H*-furo[2,3-c]pyran-2-one[4]. Its analogs were subsequently discovered and shown to comprise a family of butenolides, which was designated karrikins (KARs)[5,6]. Recent studies demonstrated that KAR signaling controls not only plant growth and development, such as the inhibition of hypocotyl elongation and inducing environmental responses[7,8], but also rhizosphere symbiosis with arbuscular mycorrhizal fungi[9].

This class of small molecules shares structural similarity with strigolactones (SLs), which are a collection of carotenoid-derived plant hormones, specifically on the butenolide moiety. It has been demonstrated that the butenolide ring is essential for retaining the bioactivity of KARs and SLs in plants[6,10]. Intriguingly, although KARs and SLs possess different physiological functions, they share a similar signaling mechanism. Both classes of compounds are first perceived by homologous α/β-hydrolase (ABH)-type receptor proteins, namely KARRIKIN INSENSITIVE2/HYPOSENSITIVE TO LIGHT (KAI2/HTL) and DWARF14/DECREASED APICAL DOMINANCE2 (D14/DAD2)[11,12]. The ligand-activated receptor KAI2 and D14 interact with MORE AXILLARY GROWTH2 (MAX2), a component of SCF-type (SKP1-CULLIN-F-box) E3 ubiquitin protein ligase complexes[13]. The SUPPRESSOR-OF-MAX2-1/(SMAX1)-LIKE (SMXL) family is subsequently targeted by MAX2 for proteasomal degradation[14–17]. Numerous studies have shown that different KAR and SL responses are triggered by the degradation of specific members of the SMAX1/SMXLs family that regulate the expression of different set of genes. In *Arabidopsis*, the activated KAI2 triggers proteolysis of two SMAX1/SMXLs family members, SMAX1/SMXL2, to mediate plant growth and development[14,15], and the destruction of three members, SMXL6/7/8, is indispensable for

[1]Graduate School of Agricultural and Life Sciences, The University of Tokyo, Tokyo, Japan. [2]Graduate School of Biostudies, Kyoto University, Kyoto, Japan. [3]Kihara Biological Institute, Yokohama City University, Yokohama, Japan. [4]Present address: School of Life Sciences, Yunnan University, Kunming, China. [5]These authors contributed equally: Jianwen Wang, Ikuo Takahashi. ✉e-mail: miyakawa.takuya.7j@kyoto-u.ac.jp; asami@g.ecc.u-tokyo.ac.jp

regulating SL response[16,17]. Nevertheless, researchers have recently found some overlap in the disruptions of certain SMAX1/SMXLs proteins triggered by KARs and SLs and thus have questioned this dichotomy[18–20]. For example, not only SMAX1/SMXL2 but also SMXL6/7/8 function to regulate root skewing in a KAI2-dependent and D14-independent manner[18], and both SLs and KARs trigger polyubiquitin-mediated degradation of SMAX1/SMXL2 to regulate hypocotyl elongation[18,19]. Moreover, in most studies, the experimentally applied SL analog GR24 is typically a racemic mixture of two enantiomers [(±)-GR24]. The 2′*R*-configured component, (+)-GR24, sufficiently activates D14, whereas its enantiomer, (-)-GR24, can elicit KAI2 signaling as that activated by KARs[21]. These systematic overlapping and similarities of the signaling system can cause much confusion when attempting to delineate the specific roles of SLs and KL. KL is the endogenous KAI2 ligand that long remain elusive[22]. Thus, there remains a demand for methods to discriminate D14 and KAI2 signaling and to find essential clues of KL.

Genetic analysis has significantly contributed to our understanding of various aspects of plant hormone signaling in the past years. Many key components of karrikin signaling, such as KAI2 and MAX2, were discovered through genetic screening. However, genetic approaches have limitations when it comes to addressing gene redundancy[23], particularly in parasitic weeds like *Striga* and *Orobanche*. These plants often possess one D14 gene and one KAI2c gene, along with multiple copies of KAI2d genes, each with diverse and still largely unknown functions. Furthermore, genetic manipulation in these parasitic plants is impractical, making it impossible to discern the specific roles of these individual proteins using genetic methods. Although Toh et al. have conducted complementation experiments in *Arabidopsis kai2* mutants, a comprehensive understanding of the roles of these proteins in their natural environment remain limited, particularly given the shared signaling components between KAR and SL.

Chemical tools provide a promising solution to this problem without introducing such intrinsic drawbacks. The use of small molecule tools, such as SL receptor agonists and antagonists, has recently led to advances in the establishment of SL biology. In this context, soporidine (SOP)[24] that inhibits ShKAI2d and *Striga* germination, has been obtained. As SOP also inhibits the germination of *Arabidopsis* induced by SL, this suggests that it lacks specificity to parasitic plants. Furthermore, given that the selectivity of SOP for AtKAI2 and AtD14 has not been reported, it is conceivable that SOP might function through the SL signal via D14 in certain physiological processes[24]. Moreover, as no specific inhibitors of AtKAI2 have been identified to date, we were prompted to develop KAI2-specific inhibitors. In this study, we present a potent and selective KAR signaling inhibitor, which we designate KK181N1. This compound blocks KAR-initiated seed germination and inhibition of hypocotyl growth. Our biochemical and crystallographic studies uncovered the inhibitory mechanism of KK181N1 on AtKAI2. Based on the characteristics of sequence variation in KAI2/HTL proteins, we proposed the structural basis for KK181N1's inhibition on KARs-activated KAI2/HTL proteins in a non-covalent binding manner, which occurs without causing cross-inhibitory activity for SLs-activated D14. This chemical would have broad applications, such as for identifying the native KL, establishing individual SL functions in plants, and most importantly, expanding our understanding of KAR/KL biology.

Results

A triazole urea compound was identified as a KAI2-signaling inhibitor

To identify potential KAI2 antagonists, we conducted a phenotype-based screening using an in-house library of triazole urea compounds (Fig. 1a)[25]. Suppression of hypocotyl elongation is one of the typical phenotypes of KAI2 signaling in *Arabidopsis*, prominently observed in response to KAI2 agonist treatment under red light conditions[26]. SL signaling also inhibits hypocotyl elongation in *Arabidopsis*, so to ensure that any observed effects were specifically due to KAI2 signaling and not SL signaling, we used an *atd14-1* mutant that is deficient in functional SL receptors[27]. In the first screening of 127 compounds, we found 9 compounds that reversed the 1 μM (±)-GR24-induced inhibition of hypocotyl elongation in the *d14-1* seedlings at 5 μM (Supplementary Figs. 1, 2a). Notably, the triazole urea compounds we prepared have two regioisomers (Supplementary Fig. 2a). These mixtures were separated by silica-gel chromatography and used to compare the inhibitory activity of the isomers. In the second screening, KAR_1 was used instead of (±)-GR24. Nine compounds demonstrated a significant ability to prevent the KAR_1-induced hypocotyl elongation inhibition in *d14-1*; the compound designated KK181N1 exhibited particularly pronounced efficacy (Fig. 1a, b and Supplementary Fig. 2b). Although the N1 isomer had more potent inhibitory activity than the N2 isomer, the hypocotyl length of the seedlings treated with 5 μM KK181N1 did not completely recover to the same degree as that of the untreated seedlings (Supplementary Fig. 2b) maybe due to the side effects of KAR_1. Next, we used KAR_2 instead of KAR_1 because it has been reported that KAR_2 is a more effective stimulant than KAR_1 in *Arabidopsis*[7]. We confirmed that KK181N1 restored the KAR_2-induced inhibition of hypocotyl elongation in a concentration-dependent manner up to 10 μM in wild-type seedlings (Fig. 1c,d). At 30 μM or higher, KK181N1 showed inhibitory effect on hypocotyl growth. The result demonstrates that KK181N1 restore the *Arabidopsis* hypocotyl elongation that was repressed by KAR-induced KAI2 signaling. In contrast, KK094, a triazole urea-type antagonist of D14[25], restored the hypocotyl length suppressed by KAR_2 at 0.3 μM, a lower concentration than KK181N1, but more dramatically shortened the hypocotyls at concentrations above 10 μM. To determine whether KK181N1 treatment produces a phenotype similar to *kai2*, the loss-of-function mutant of KAR signaling, we assessed the impact of KK181N1 treatment alone on hypocotyl elongation. Solo treatment with KK181N1 did not cause hypocotyl elongation like *kai2* mutant in wild-type seedlings, but rather suppressed it above 30 μM (Supplementary Fig. 3a), indicating that high concentrations of KK181N1 result in the suppression of seedling growth due to side effect. It should be mentioned that these results do not rule out the possibility that such side effects may mask the compound's antagonistic effect on endogenous KL reception. Consequently, we did not obtain clear evidence that KK181N1 disrupts endogenous KL-activated KAI2 signaling during hypocotyl growth.

It has been reported that enhanced KAI2 signaling restores the seed germination ability that is suppressed under high-temperature conditions[28]. As expected, we found that KK181N1 inhibited the recovery of seed germination ability by KAR_2 after exposure to high temperatures. While KK094 showed inhibition only at 100 μM, the potency of KK181N1 for this inhibitory activity was significant at concentrations above 3 μM (Fig. 1e). Solo treatment of KK181N1 under high-temperature condition had no clear effect on seed germination in wild-type. However, under ambient temperature conditions, KK181N1 concentrations exceeding 30 μM were observed to inhibit wild-type seed germination (Supplementary Fig. 3b, c). To distinguish whether the inhibition of germination by KK181N1 was due to side effects distinct from disturbance of KAR signaling, the effect of KK181N1 treatment alone in the *kai2* mutant was also assessed. In the *kai2* mutant, as in wild-type, KK181N1 concentrations above 30 μM showed inhibitory activity under ambient temperature conditions (Supplementary Fig. 3d, e). This indicates that KK181N1 concentrations above 30 μM suppress seed germination in a KAI2-independent manner. These results suggest that KK181N1 suppresses seed germination by disrupting exogenous KAR-activated KAI2 signaling.

Since KK181N1 is structurally similar to KK094, we next evaluated its preference for KAI2 using *Arabidopsis kai2-2*, *atd14-1*, and *max2-1* mutants, and *atd14kai2* double mutant[27,29]. The *atd14kai2* and *max2-1* mutants correspond to deficiencies in both KAR and SL signaling

https://doi.org/10.1038/s41467-024-54801-1

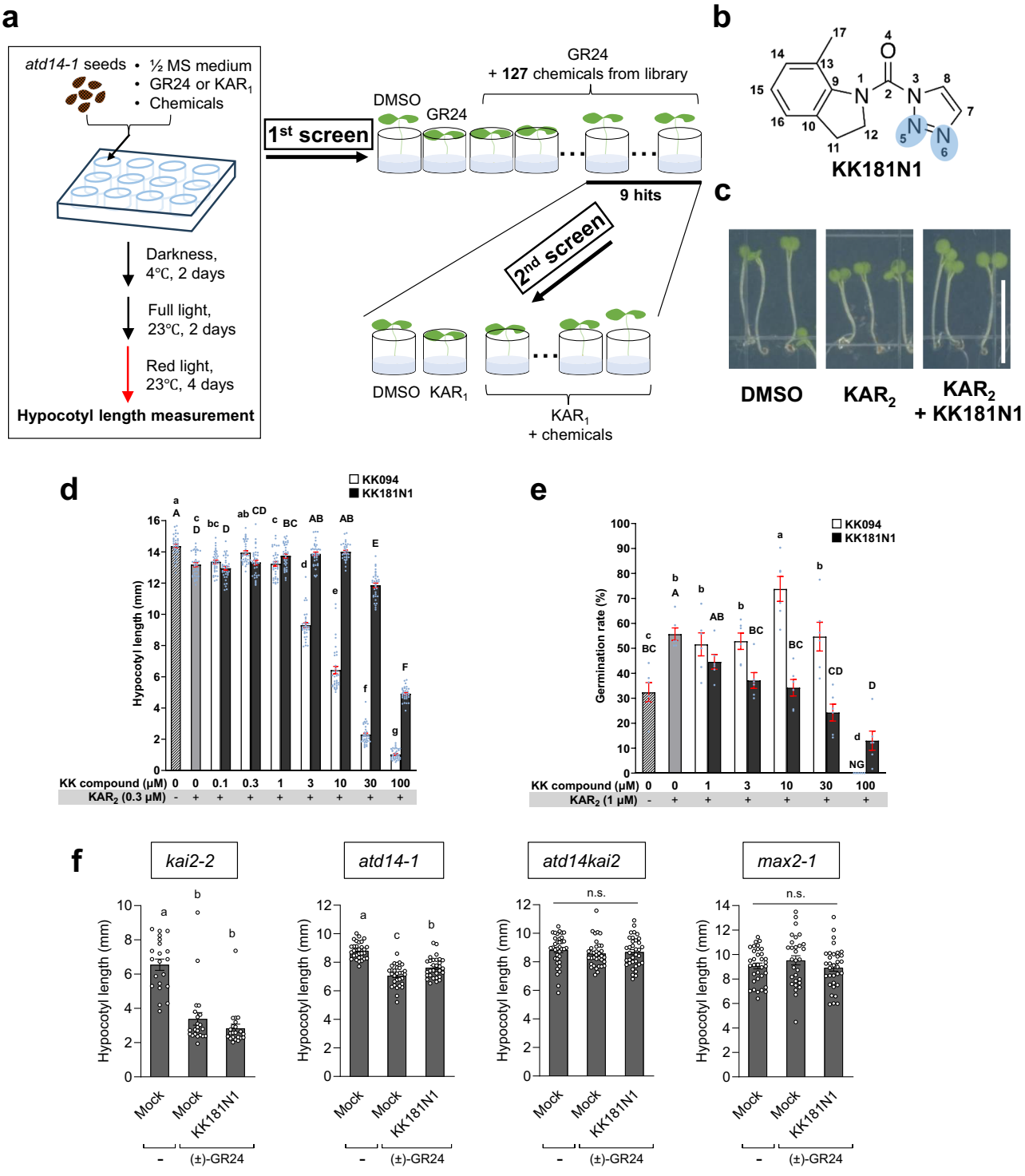

transduction pathways. (±)-GR24 causes inhibition of hypocotyl growth through KAR and SL signaling. If KK181N1 is selective for KAI2 signaling, we expected this compound to recover the (±)-GR24-inhibited hypocotyl growth only in the *atd14-1* mutant because KAI2 signal functions only in this mutant among them. The results showed that co-treatment of KK181N1 and (±)-GR24 did not make morphological changes to the hypocotyls of the *atd14kai2* and *max2-1* mutants, suggesting that KK181N1 effects are MAX2-dependent (Fig. 1f). Moreover, we observed that treatment with KK181N1 partially recovered (±)-GR24-induced growth inhibition in the *atd14-1* mutant, but not in the *kai2-2* mutant, indicating that KK181N1 may suppress only KAI2 function, not D14 function (Fig. 1f). Collectively, these results suggest that KK181N1 is a KAI2-signaling inhibitor that did not interfere with SL signaling.

KK181N1 binds to the catalytic pocket of AtKAI2

KK181N1-induced phenotypes in *Arabidopsis* seeds and hypocotyls were similar to those of the *kai2-1* mutant[27], suggesting that KK181N1 might directly target KAI2. Therefore, we estimated the affinity of KK181N1 for purified recombinant *Arabidopsis* KAI2 (AtKAI2) using isothermal titration calorimetry (ITC) (Supplementary Fig. 4a, b). The binding affinity (indicated by a dissociation constant, K_d) of AtKAI2 to

Fig. 1 | Screening to identify a KAI2 signaling inhibitor. a Schematic diagram of the screening using an in-house chemical library to identify KAI2 signaling inhibitor(s). *Arabidopsis* seeds of *atd14-1*, which is an SL receptor disruption mutant, were used in this screening. In the first step of the screening, the seeds were co-treated with 1 μM (±)-GR24 and 127 chemicals (5 μM each) from our in-house library. Nine chemical hits that reversed (±)-GR24-induced hypocotyl inhibition were further tested in the second step of the screening, where the seeds were co-treated with 1 μM KAR_1 and 9 candidate chemicals (5 μM each). **b** Chemical structure of KK181N1 with atom numbering. Two nitrogen atoms in the 1,2,3-triazole moiety are highlighted in blue. **c** Representative seedlings of 7-d-old wild-type *Arabidopsis* grown on MS medium containing 0.3 μM KAR_2 co-treated with DMSO or 10 μM KK181N1. DMSO is the mock control. Scale bar = 10 mm. **d** Hypocotyl growth of wild-type *Arabidopsis* seedlings in response to 0.3 μM KAR_2 supplemented with different concentrations of KK094 (white column) and KK181N1 (black column). Hypocotyl length was measured after cultivation under fluorescent white light (30 μmol m^{-2} s^{-1}) at 22 °C for 2 days followed by under red LED light (35 μmol m^{-2} s^{-1}) at 22 °C for 4 days. Values and bars represent the means ± SE (n = 35 (0 μM KAR_2, 0.3 μM KAR_2 + 3 μM KK094, 0.3 μM KAR_2 + 10 μM KK094, 0.3 μM KAR_2 + 0.3 μM KK181, 0.3 μM KAR_2 + 10 μM KK181, 0.3 μM KAR_2 + 30 μM KK181, and 0.3 μM KAR_2 + 100 μM KK181), 36 (0.3 μM KAR_2, 0.3 μM KAR_2 + 0.3 μM KK094, 0.3 μM KAR_2 + 1 μM KK094, 0.3 μM KAR_2 + 1 μM KK181), 37 (0.3 μM KAR_2 + 0.1 μM KK094, 0.3 μM KAR_2 + 0.1 μM KK181), 38 (0.3 μM KAR_2 + 100 μM KK094), and 39 (0.3 μM KAR_2 + 30 μM KK094)). Letters indicate significant differences ($P < 0.05$), as determined by one-way ANOVA followed by two-tailed Tukey's HSD test for multiple-pair comparisons. **e** The germination rate of wild-type *Arabidopsis* seeds co-treated with 1 μM KAR_2 and different concentrations of KK094 (white column) and KK181N1 (black column) was recorded. The seeds were first incubated at 30 °C under continuous fluorescent white light (20 μmol m^{-2} s^{-1}) for 48 h and then at 22 °C for an additional 48 h. Data are the results of 6 biological replicates of around 30 seeds each. Values and bars represent the means ± SE. Letters indicate significant difference ($P < 0.05$), as determined by one-way ANOVA followed by two-tailed Tukey's HSD test for multiple-pair comparisons. **f** Hypocotyl growth of *Arabidopsis kai2-2*, *atd14-1*, *atd14kai2* and *max2-1* seedlings in response to 1 μM (±)-GR24 supplemented with DMSO or 5 μM KK181N1. Hypocotyl length was measured after cultivation under fluorescent white light (30 μmol m^{-2} s^{-1}) at 22 °C for 2 days followed by under red LED light (35 μmol m^{-2} s^{-1}) at 22 °C for 4 days. Values and bars represent the means ± SE (n = 21) (Mock in *kai2-2*), 22 (Mock + 1 μM (±)-GR24 and 5 μM KK181 + 1 μM (±)-GR24 in *kai2-2*), 30 (Mock, Mock + 1 μM (±)-GR24, and 5 μM KK181 + 1 μM (±)-GR24 in *d14-1*, and Mock + 1 μM (±)-GR24 in *max2-1*), 33 (5 μM KK181 + 1 μM (±)-GR24 in *max2-1*), 34 (Mock in *max2-1*), (Mock + 1 μM (±)-GR24, and 5 μM KK181 + 1 μM (±)-GR24 in *d14kai2*), and 36 (Mock in *d14kai2*). Letters indicate significant difference ($P < 0.05$), as determined by one-way ANOVA followed by two-tailed Tukey's HSD test for multiple-pair comparisons. n.s. indicates not significant. Source data are provided as a Source Data file.

KK181N1 was 27.7 μM (Fig. 2a), which is stronger than that of AtKAI2 to KAR_1 (129 or 147.5 μM)[30,31].

To elucidate the binding site and mode of KK181N1 in AtKAI2, we determined the crystal structure of AtKAI2 in complex with KK181N1 at 1.9 Å resolution (Supplementary Table 1). Three protein molecules were detected in an asymmetric unit of the AtKAI2-KK181N1 crystals (Supplementary Fig. 4c). These molecules were essentially identical, with root-mean-square deviation (RMSD) values of 0.11–0.25 Å for the main chain C_α atoms when the overall structures were superimposed pairwise (Supplementary Fig. 4d). Unlike KK094, which covalently bound to OsD14[32], the intact KK181N1 molecule was found to be embedded near a catalytic residue S95 of AtKAI2, as evidenced by the clear electron density map (Fig. 2b). The residues lining the catalytic pocket bring multiple polar and non-polar interactions (within 5 Å) to firmly envelope the entire KK181N1, including F26, S95, V96, Y124, F134, L142, F157, A161, F174, I193, F194, L218, A219, and H246 (Fig. 2c–e and Supplementary Fig. 5).

At the bottom of the catalytic pocket, four water molecules (W1, W2, W3, and W4) are trapped by mediating a hydrogen-bonding network (Fig. 2b). This network connects to the 1,2,3-triazole ring of KK181N1, the amide backbone of F26 and V96, and the hydroxy group of S95, S119, and Y124 (Fig. 2c). S95 plays a crucial role in this hydrogen-bonding network by forming multiple hydrogen bonds with two water molecules (W3 and W4) and the 1,2,3-triazole ring of KK181N1. As reported previously, serine, cysteine, and aspartic acid all work as the catalytic nucleophile in the ABH fold[33]. In ITC experiments, the mutants S95C and S95D still showed 97% and 65% of the KK181N1-binding affinity of the wild type, respectively, while the affinity of S95A toward KK181N1 was barely detectable (Fig. 2f, Supplementary Fig. 6 and Supplementary Table 2). Even though one of the catalytic triad residues, D217, does not directly interact with KK181N1, its carboxy group forms two hydrogen bonds with the imidazole ring of H246 and the amide backbone of A219 to stabilize the binding with KK181N1 (Fig. 2c). Both mutants D217A and D217E almost lost KK181N1-binding affinity (Fig. 2f). H246 and A219 are involved in establishing the hydrophobic pocket to recognize the body of KK181N1 (Fig. 2c). The imidazole ring of H246 also directly engages in the core hydrogen-bonding network by forming a hydrogen bond with S95. The mutants H246A and H246F showed about 30% binding affinity to KK181N1 (Fig. 2f). These results revealed that the water-mediated hydrogen-bonding network and the formation of the S95-H246-D217 catalytic triad are crucial for anchoring KK181N1 at the bottom of the catalytic pocket.

In the middle and bottom of the catalytic pocket, KK181N1 interacts with several hydrophobic residues, including F26, Y124, A161, F174, I193, F194, and A219 (Fig. 2d and Supplementary Fig. 5a,c). ITC assay of alanine-substituted mutants demonstrated that residues with bulkier hydrophobic side chains among these amino acids significantly contribute to the binding of KK181N1 (Fig. 2f, Supplementary Fig. 6 and Supplementary Table 2). The mutants F157A, F174A, and F194A showed minimal (<10%) or no binding activity, and variants F26A and I193A only maintained low (10–36%) or moderate (71%) affinity to KK181N1, respectively (Fig. 2f).

The other hydrophobic residues—F134, L142, and L218—are located near the entrance of the catalytic pocket and interact with the hydrophobic edge of the 7-methylindoline moiety of KK181N1. The binding affinity of these alanine mutants to KK181N1 was dramatically increased (Fig. 2f, Supplementary Fig. 6 and Supplementary Table 2). Given that KK181N1 is tightly embedded by the water-mediated hydrogen-bonding network at the bottom of the pocket and the hydrophobic interactions at the middle of pocket (Fig. 2c,d), we inferred that these three pocket entrance-lining residues, typically called gatekeeper residues, may function solely as guardians for ligand entry (Fig. 2e), which means that alanine substituent at these positions would enlarge the pocket entrance to accelerate the association/dissociation of KK181N1 without interfering with ligand recognition. To support this hypothesis, we prepared four more variants of L218 that were substituted with V/I/F/Y. As presumed, L218V and L218I possessed slightly decreased KK181N1-binding affinity compared with L218A, although their KK181N1-binding affinities were still higher than that of the wild type. In contrast, L218F and L218Y showed a complete loss of binding affinity to KK181N1 (Fig. 2f), probably due to the partial or complete coverage of the pocket entrance, leading to the rejection for ligand entry by their bulky side chain. Consistent with the structural information, the results of the affinity assay indicate that the hydrogen-bonding network located at the bottom of the pocket and the hydrophobic walls built by the non-polar residues both significantly contribute to the embedding of KK181N1 within the pocket. The results also show that releasing hydrophobic effect at the entrance will promote the recognition of KK181N1.

Binding of KK181N1 is fine-tuned by conformational changes in some hydrophobic residues

To investigate the conformational changes of AtKAI2 upon binding of KK181N1, we compared the structure of the AtKAI2-KK181N1 complex

https://doi.org/10.1038/s41467-024-54801-1

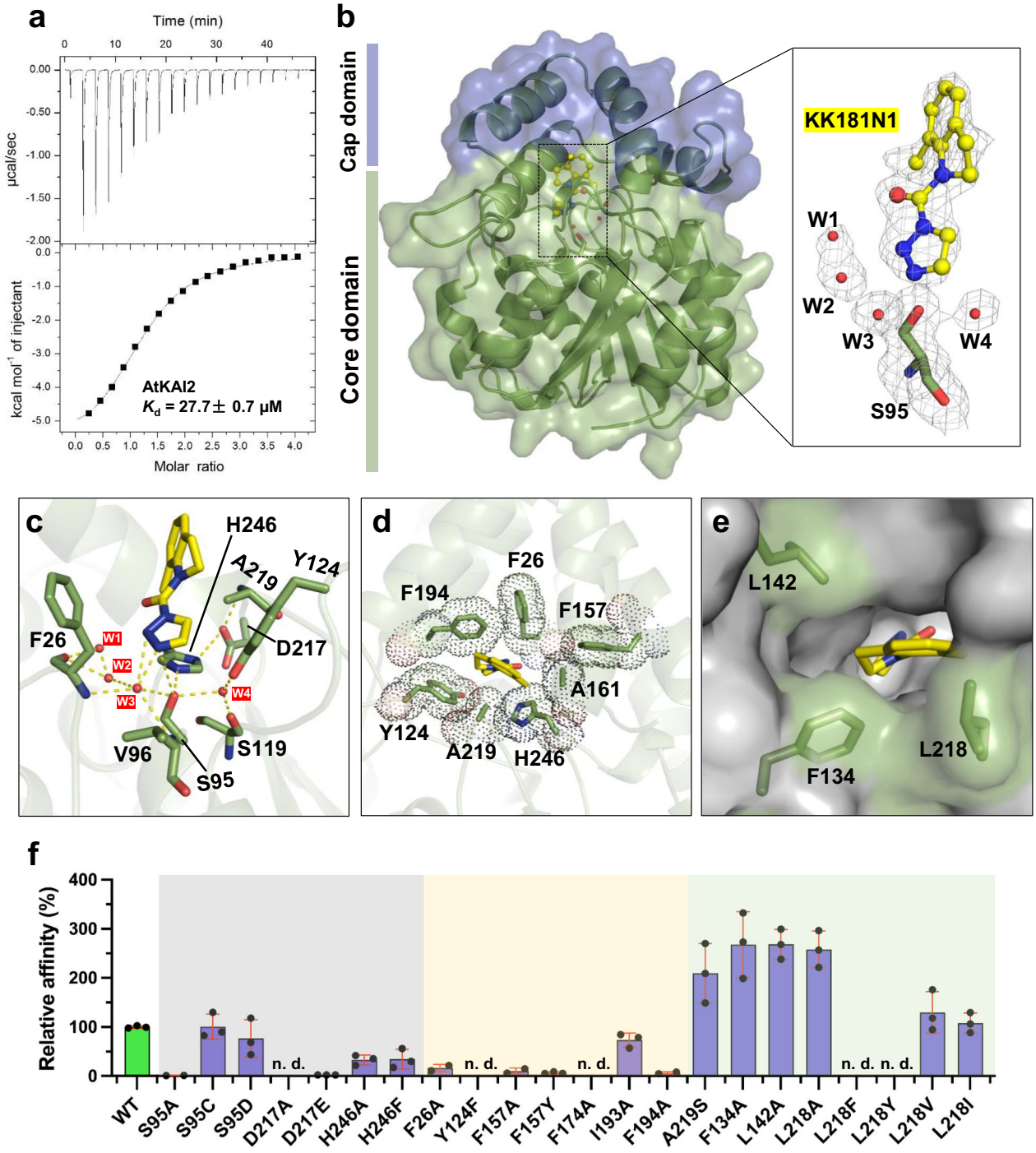

Fig. 2 | Recognition of KK181N1 by AtKAI2. a ITC thermograms from the titration of KK181N1 into AtKAI2. Binding of KK181N1 to AtKAI2 gave a dissociation constant (K_d value) of 27.7 ± 0.4 µM, as calculated from three independent experiments. Error bar indicate standard deviation (SD) (n = 3 technical replicates). **b** Crystal structure of AtKAI2-KK181N1. The structure is represented with ribbon and surface models. The cap domain is colored purple, and the core domain is green. In the close-up view of the active site of AtKAI2, KK181N1 (shown as a yellow sphere) is non-covalently embedded in the catalytic pocket. The relative spatial positions of catalytic nucleophile S95 (shown as the green stick) and four water molecules (named W1 to W4 and shown as red spheres) situated at the bottom of the pocket to KK181N1 are presented, along with the F_o-F_c omit map contoured at 2.0 σ (gray). **c** The hydrogen-bonding network formed at the bottom of active site. The residues involved in this network are shown as green stick models. Hydrogen bonds are shown as dashed yellow lines. **d** The hydrophobic interaction of KK181N1 with residues situated in the middle part of the pocket. Residues are represented as green sticks and further covered with dots to indicate the atomic surface with van der Waals radius. **e** Three residues (F134A, L142A, and L218A) along the boundary of the pocket are indicated. **f** The binding affinity of KK181N1 to AtKAI2 with mutations of pocket residues was measured by ITC. The relative affinity was calculated with K_d values for comparisons among mutants. n. d. indicates not detected. The gray, light orange, and light green shading respectively represent the relative affinity of residues with mutation at the bottom, middle, and entrance of the pocket. Data are means of 2–4 technical replicates. ITC thermograms for each mutant are shown in Supplementary Fig. 6. A summary of K_d values is given in Supplementary Table 2. Source data are provided as a Source Data file.

with those of the *apo*-AtKAI2 (PDB code: 4JYP)[34] and AtKAI2-KAR_1 complexes (PDB code: 4JYM)[34], resulting in RMSD values of 0.188 Å and 0.196 Å for the main-chain C_α atoms, respectively (Supplementary Fig. 7a). The structural data showed that the overall structure of AtKAI2 was quite similar among the three states, and KK181N1 binding did not induce a large conformational change.

We found that KK181N1 induces slight conformational shifts of residues F157 and L142, while KAR_1 does not (Supplementary Fig. 7d,e). The most pronounced conformational changes were observed on the side chains of F194 and L218 (Supplementary Fig. 7f–h). For F194, the binding of KK181N1 and KAR_1 causes conformational changes to almost the same degree, where the benzene ring of F194 rotates outward 79° to escape the steric hindrance with the ligand body and to further establish π-π stacking interactions with the 4*H*-pyran of KAR_1 in the face-to-face geometry or with triazole of KK181N1 in the parallel displaced orientations (Supplementary Fig. 7f). Notably, the C_β-C_γ bond of L218 rotates 134° upon KAR_1 binding (Supplementary Fig. 7g) but causes dihedral turns of over 163° along with a 1.7 Å shift of C_γ upon KK181N1 binding (Supplementary Fig. 7h). This is remarkably consistent with our affinity assay for L218 mutants, in which L218A/V/I showed stronger binding affinity to KK181N1 than the wild type did (Fig. 2f). Collectively, these structural details inform us that some conformational changes will be required to improve the binding with KK181N1.

KK181N1 is a selective non-covalent inhibitor of KAI2

Previously, we identified an SL receptor antagonist, KK094, that targets D14, the paralogue of KAI2[25]. In the rice D14 (hereafter OsD14)-KK094 complex structure, the KK094-derived carbamoyl moiety (KK094CM) covalently attaches to the hydroxy group of the nucleophile S147. To form a covalent bond, the side chain of S147 must rotate toward the ligand by 27° (Supplementary Fig. 8a, b), whereas the orientation of S95 in *apo*-AtKAI2 essentially resembles that in AtKAI2-KAR_1 and AtKAI2-KK181N1 (Supplementary Fig. 7c).

KK094 and KK181N1 exhibit distinct binding modes in OsD14 and AtKAI2, respectively, although they differ by only one methyl group in the indole ring. In the catalytic pocket of AtKAI2, five residues (F157, A161, L218, A219, and H246) provide hydrophobic and/or CH/π interactions with the methyl group of KK181N1 (Supplementary Fig. 8c, d). Among them, three residues (F157, L218, and A219) are divergent in OsD14, corresponding to Y209, V269, and S270, respectively. The structural overlay indicates that the hydroxy group of Y209 (OsD14) causes a steric hindrance both on the carbonyl and the methyl groups of KK181N1 (Fig. 3a), whereas V269 (OsD14) may not interfere with KK181N1 binding (Supplementary Fig. 9a). KK181N1 also avoids causing any steric hindrance with S270 (the ligand-free state of D14) by rotating its hydroxy group over 130° outwards in the pocket (Supplementary Fig. 9b). These structural features explain the results that KK181N1-binding affinity was promoted by the single point mutations L218V and A219S but was attenuated by F157Y (Fig. 3b and Supplementary Fig. 9c, d). However, a similar binding affinity of KK181N1 was observed for both AtKAI2 and Os/AtD14 (Fig. 2a and Supplementary Fig. 10). This is likely because of the synergistic interactions of multiple residues in ligand binding, where detrimental mutations can be offset by beneficial ones. For example, for KK181N1 binding in OsD14, the negative impact of the Y209 mutation might be counteracted by beneficial residues such as V269 and S270.

In the bottom of the pocket, Y124 stabilizes the binding of KK181N1 not only through the π-π interaction but also through the water-mediated hydrogen bond (Figs. 2c, 3c). However, no binding of $AtKAI2^{Y124F}$ to KK181N1 was detected (Fig. 3d), which suggests that the formation of a water-mediated hydrogen bond is a more critical role of Y124 for KK181N1 binding of AtKAI2. Previous studies have also suggested that Y124 is a key residue for the structural divergence between KAI2/HTL and D14 proteins[35], because the hydroxy group of Y124 occludes a pocket adjacent to the substrate-binding cavity, whereas substitution of the D14 residue corresponding to Y124 in AtKAI2 for F prevents the bisection of pockets, resulting in a substrate-binding cavity large enough to accommodate SL (Fig. 3c). Although ITC data showed the binding affinity of KK181N1 was nearly identical between AtKAI2 and Os/AtD14s, their thermodynamic patterns were different. AtKAI2, in which Y124 is incorporated, showed the highest enthalpic binding mode, which may support the water-mediated hydrogen bonds (Figs. 2a, 3c). Thus, the binding pattern of KK181N1 may be different between AtKAI2 and D14s. Moreover, many models of parasitic KAI2 proteins have also suggested that KAI2d containing smaller amino acid substitutions at this position had a larger ligand-binding pocket than KAI2c and KAI2i, and showed morphology more similar to OsD14 than AtKAI2[35]. Thus, the smaller pocket size defined by Y124 may contribute to the fixed placement of KK181N1 at the position identified in the crystal structure of the AtKAI2-KK181N1 complex.

To confirm that KK181N1 is a potential selective inhibitor of KAR signaling, we first investigated whether KK181N1 induces bud outgrowth of rice, since the *d14* mutant and KK094-treated rice have an increase in the number of tillers with dwarfism[25]. KK181N1 did not show an increased tiller number but did show stunted plant height (Supplementary Fig. 11a–c). Next, we examined the inhibitory effect of KK181N1 on seed germination in a root parasitic *Orobanchaceae*, *Striga hermonthica*. *Orobanchaceae* parasites KAI2/HTL have undergone a considerable evolutionary expansion of the *KAI2* gene family and have been classified into three clades: KAI2i, KAI2c, and KAI2d (Supplementary Fig. 11a)[35]. Their seed germination is regulated by a KAI2d-mediated signal with a strong preference for SL rather than for KARs[35]. We found that KK181N1, when applied with 10 nM (±)-GR24, failed to block SL-induced seed germination even at 100 μM (Fig. 3e). Among three clades of KAI2 proteins in *S. hermonthica* (ShKAI2s), even though ShKAI2c/ShHTL1, which contains Y124 at this position, can bind with KARs (Fig. 3f)[30], its biological function remains unknown[35]. ShKAI2d6/ShHTL7 is the main receptor for regulating seed germination with hypersensitivity to SL and has a substituted Leu residue at the position corresponding to AtKAI2 Y124[36]. Therefore, this residue difference may be one of the reasons why KK181N1 cannot obstruct SL-stimulated seed germination. Indeed, KK181N1 showed an inhibitory effect on seed germination of lettuce (Fig. 3g), which probably occurred through KAR_1-activated LsKAI2a but not LsKAI2b because LsKAI2b contains a phenylalanine substituent at this position (Fig. 3f). These results indicated that KK181N1 has selective and inhibitory biological activity against KAR-activated signals in specific plant species.

AtKAI2 possesses intact catalytic triad residues and shows hydrolysis activity against (-)-GR24[37,38]. To answer why AtKAI2 did not hydrolyze KK181N1 as OsD14 did to KK094, we modeled the methyl group on the KK094CM (termed Methyl-KK094CM) (Fig. 3h). It can be clearly seen that the additional methyl group causes a severe steric clash with the side chains of F78 and V244 in OsD14, which respectively correspond to F26 and I193 in AtKAI2. This suggests that F26 and I193 of AtKAI2 is a critical residue for the non-covalent binding mode of KK181N1 to AtKAI2. Moreover, it is likely that the methyl group of KK181N1 also assists in preventing the binding orientation of itself in a covalent manner in the pocket of AtKAI2, because, as mentioned above, five residues provide tight interactions with the methyl group of KK181N1 (Supplementary Fig. 8d). We further tested an array of derivatives that have different substitutions on the methyl of KK181N1 (Fig. 3i). However, all of them displayed the alleviated affinity for AtKAI2, just as they showed decreased inhibitory activity for *Arabidopsis* (Supplementary Fig. 2b). Taken together, these results suggest that the methyl group is the most suitable substitution group for a KK181N1-like inhibitor of KAI2 with a non-covalent mode of action.

Water-mediated hydrogen bonding network shows selectivity for N-heterocyclic urea compounds

As described above, the four water molecules at the bottom of the catalytic pocket play a crucial role in the noncovalent binding with

https://doi.org/10.1038/s41467-024-54801-1

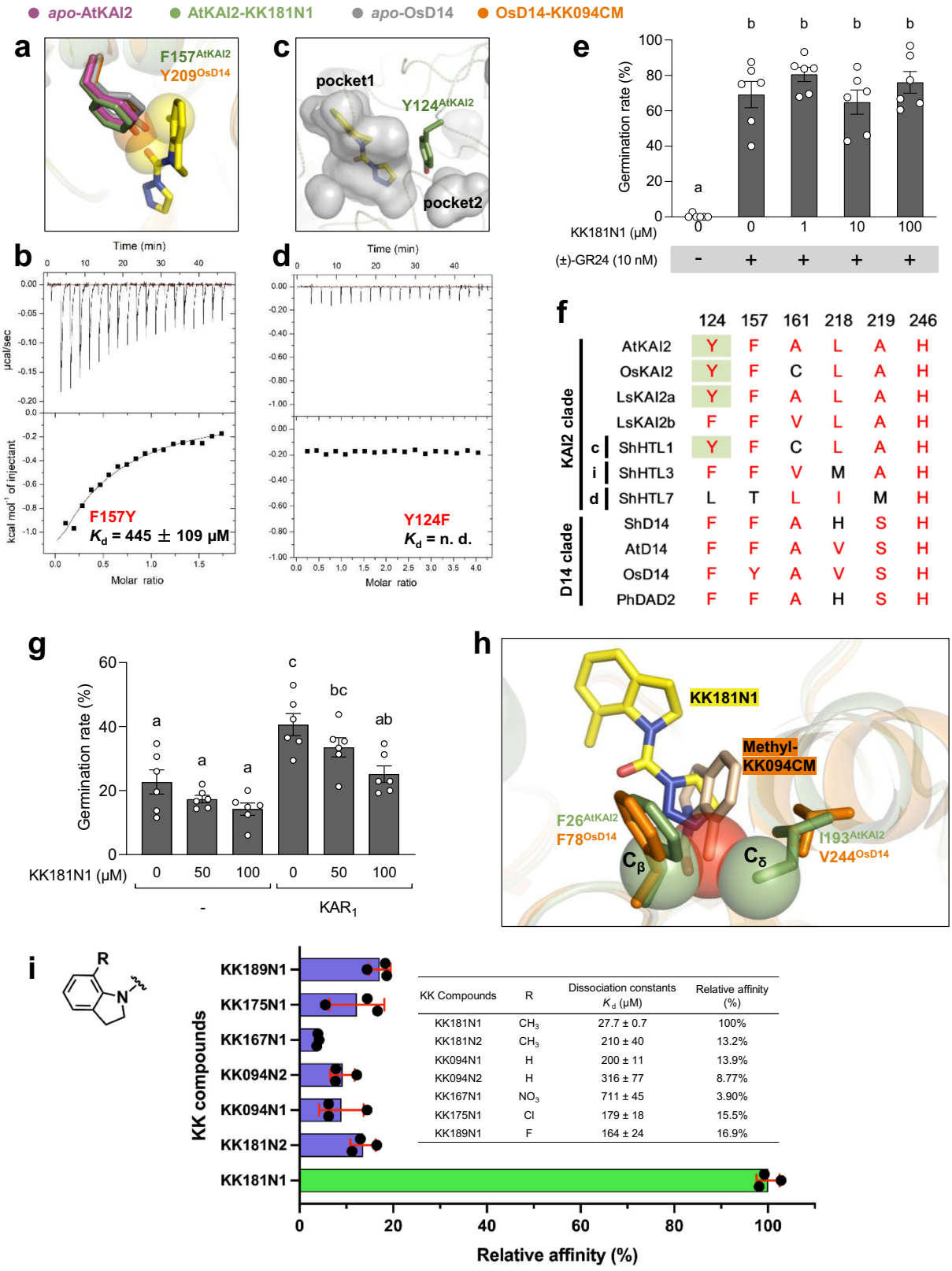

KK Compounds	R	Dissociation constants K_d (µM)	Relative affinity (%)
KK181N1	CH_3	27.7 ± 0.7	100%
KK181N2	CH_3	210 ± 40	13.2%
KK094N1	H	200 ± 11	13.9%
KK094N2	H	316 ± 77	8.77%
KK167N1	NO_3	711 ± 45	3.90%
KK175N1	Cl	179 ± 18	15.5%
KK189N1	F	164 ± 24	16.9%

KK181N1 by forming a hydrogen bonding network (Figs. 2c, 4a). On the other hand, the covalent binding with KK094 in OsD14 required two water molecules positioned differently from those in the AtKAI2-KK181N1 complex (Fig. 4b)[25]. These two water molecules in OsD14-KK094CM constitute the hydrogen-bonding network between W1, W2, and the amide backbone of F78 and further extend to the hydroxy group of Y209 (F157 in AtKAI2) (Fig. 4b). In both cases, water molecules seem to support the bonding with KK compounds by placing them in the proper positions. More interestingly, the hydrogen-bonding networks in OsD14-KK094CM and AtKAI2-KK181N1 are essentially bridged by the backbones of F26/78 and V96/148, the residues that form the oxyanion hole in the catalytic reaction of ABH (Fig. 4a,b). In AtKAI2-KK181N1, KK181N1 is indirectly stabilized by the main chain amides of F26 and V96 through the establishment of two hydrogen bonds with

Fig. 3 | Structural basis for KK181N1 as the KAI2-specific non-covalent antagonist. a Structural comparison of residue F157 in *apo*-AtKAI2 (PDB code: 4JYP, magenta) and AtKAI2-KK181N1 (this study, green) with Y209 in *apo*-OsD14 (PDB code: 3VXK, gray) and OsD14-KK094CM (PDB code: 5ZHR, orange). KK181N1 is indicated by a cyan stick. Sphere models show oxygen atoms with the van der Waals radius. **b** ITC thermograms of the AtKAI2 mutant F157Y, producing a weak affinity with a K_d value of 445 ± 109 µM. Data are means ± SD (n = 3 technical replicates). **c** The active site of AtKAI2 was separated into two pockets (1 and 2) by residue Y124. The cavities are shown as a semitransparent surface. **d** ITC thermograms of the AtKAI2 mutant Y124F. The K_d value is not detected (n. d.). **e** The germination rate of *Striga hermonthica* seeds treated with 10 nM (±)-GR24 and DMSO or different concentrations of KK181N1 was recorded. The conditioned seeds were applied compounds and incubated at 30 °C in the dark for 2 days. Data are the results of 6 biological replicates of around 50 seeds each. Values and bars represent the means ± SE. Letters indicate significant difference (P < 0.05), as determined by one-way ANOVA followed by two-tailed Tukey's HSD test for multiple-pair comparisons. **f** Sequence alignment of Y124 and residues interacting with the methyl group of KK181N1. c, i, and d respectively represent the conserved, intermediate, and divergent subclades of parasitic HTLs proteins. Full sequence alignment is shown in Supplementary Fig. 14. **g** The germination rate of lettuce seeds treated with different concentrations of KK181N1 in the presence and absence of 1 µM KAR_1. The seeds were incubated at 22 °C in the dark for 48 h. Data are the results of 6 biological replicates of around 50 seeds each. Values and bars represent the means ± SE. Letters indicate significant difference ($P < 0.05$), as determined by one-way ANOVA followed by two-tailed Tukey's HSD test for multiple-pair comparisons. **h** Structural comparison of AtKAI2-KK181N1 (green) and OsD14-KK094CM (PDB code: 5ZHR, orange). The van der Waals radius is indicated by spheres. The methyl group (red spheres) was modeled on KK094CM by PyMOL 2.5.4, producing Methyl-KK094CM. This hypothetical methyl group is thought to cause strong steric hindrance with C_β of F26 and C_δ of I193 (green spheres). **i** The binding affinities of AtKAI2 to 1,2,3-triazole ureas were measured by ITC assays. The relative affinity is calculated with K_d values (in the Table) for the comparisons among compounds. Data are means of 2 or 3 technical replicates (mean ± SD). ITC thermograms are shown in Supplementary Fig. 13. The chemical structures of 1,2,3-triazole ureas are shown in Supplementary Fig. 2a. Source data are provided as a Source Data file.

the water molecule (W3) (Fig. 4a). In the case of KK094CM, the carbonyl group was nearly superimposed with the water molecule (W3) in AtKAI2 and directly forms hydrogen bonds with the main chain amides of F26 and V96 (Fig. 4b). Hence, we hypothesize that this oxyanion hole plays an important role in capturing and precisely positioning water molecules, thereby facilitating the anchoring of KK compounds at the bottom of the catalytic pocket of KAI2/D14.

KK181N1 connects to this water-mediated hydrogen-bonding network through its 1,2,3-triazole moiety, where one of three nitrogen atoms (termed N5, a hydrogen acceptor; Fig. 1b) forms a hydrogen bond with a water molecule (W3), and another nitrogen atom (termed N6, a hydrogen donor) forms two hydrogen bonds, respectively, with W3 and the hydroxy group of S95 (Fig. 4a and Supplementary Fig. 5a). A similar architecture was observed in OsD14–KK09CM interactions, where the covalent bonds link the carbonyl oxygen and indoline nitrogen of KK094CM with the hydroxy group of S147 (Fig. 4b).

1,2,3-triazole-containing compounds have N1- and N2-carbamoylated regioisomers (Supplementary Fig. 2a). The affinity assay demonstrated that AtKAI2 exhibited a preference for KK181 containing N1 regioisomers (Fig. 3i). This is probably because the N2-configured 1,2,3-triazole forms one hydrogen bond between an N5 atom and a water molecule (W3), which is weaker than the two hydrogen bonds built by an N6 atom (Fig. 4a), and therefore the N1-configured 1,2,3-triazole has an higher affinity than the N2-configured compounds. To confirm this result, we first prepared KK122, which replaced 1,2,3-triazole with imidazole in KK094. As expected, even in the absence of an N5 atom, the harboring of N6 in KK122 reinforced the binding affinity so that it was approximately 3-fold higher than that of KK094N2, or 2-fold higher than that of KK181N2, demonstrating that N6 atom-formed hydrogen bonds are vitally crucial for the binding affinity of 1,2,3-triazole-containing chemicals toward AtKAI2 (Figs. 3l, 4c,d and Supplementary Fig. 13). However, when we replaced the N-heterocyclic moiety of KK122 with furan, the produced chemical KK200 showed decreased affinity to AtKAI2 (Fig. 4d). Unexpectedly, KK122 exhibited a higher AtKAI2-binding affinity than KK094N1. We also prepared KKT3054, which contains an additional methyl group in KK122. ITC measurement showed that, compared with KK181N1, KKT3054 has a stronger binding affinity to AtKAI2, possibly due to the desolvation penalty that the ligand suffered when it bound to the receptor, which is more pronounced in triazole-containing compounds with higher solubility[39,40]. Consequently, the hydrogen bonds formed by the triazole moiety, and particularly by its N5 atom, could not compensate for the free energy loss of desolvation, with the result that this hydrogen bond made no contribution to the binding affinity of the receptor. KKT3054 also presented more potent inhibitory activity than KK181N1 on KAR_1-induced hypocotyl elongation and seed germination in *Arabidopsis* (Fig. 4e,f).

Taken together, our results showed that the conserved hydrogen-bonding network among D14 and KAI2 proteins is crucial for capturing N-heterocyclic urea inhibitors, whether through covalent or non-covalent interactions. Moreover, the N1-configured 1,2,3-triazole moiety can strengthen the water-mediated hydrogen-bonding network, increasing its binding affinity.

Discussion

KARs and SLs, two families of butenolide compounds, are crucial signaling molecules with distinct roles in the regulation of many aspects of plant growth and development. Here, we present an inhibitor of AtKAI2 that solely exhibits an antagonistic effect on KARs-signaling. We further provide structural insight into the actions of KK181N1 on AtKAI2, revealing the structural basis of its high sensitivity.

Our triazole ureas-based in-house chemical library is designed to target ABH-type macromolecules of plants with tunable selectivity. KAI2 and D14 are both subject to the ABH superfamily and function to preserve the canonical arrangement of a catalytic triad Ser-His-Asp for ligand perception, and therefore they have the potential to be targeted by covalent probes. From this chemical library, we previously identified several SL antagonists that covalently bind to D14, an SL receptor. The AtD14-CLIM-D3 structure complex reveals an open-to-closed conformational transition for the signaling activation of SLs[11]. We initially considered that the mode of action of covalent triazole urea antagonists (such as KK094CM) is to occupy the active site of D14 by means of a solid covalent interaction, and the covalently bound moiety of the antagonists may be too large to allow the lid collapse required for the interaction with the downstream protein, D3. However, our results revealed that KK181N1 has a well-fitting non-covalent binding mode at the active site of AtKAI2. Compared with KAR_1, KK181N1 had higher affinity to AtKAI2[30]. These observations suggest that KK181N1 and KARs might compete for the same ligand site on KAI2. A notable recent study by Arellano-Saab et al. revealed the structure of strigolactone-bound ShHTL5, showing strong electron density corresponding to the intact SL structure. This study suggested that the essential D-ring of SL in ShHTL5 shares a similar binding position with a D-ring hydrolysis product complexed to D14[41]. Although some research suggests that KARs are metabolized into an active signal (KL) instead of being directly recognized by KAI2, we propose that KARs metabolites could also share a similar binding mode to KARs, particularly concerning their butenolide moiety. This implies that KK181N1 competes with both KARs and their metabolites for binding interactions. Such a non-covalent binding of KK181N1 could cause the conformational changes on the protein interface, ultimately interfering with/blocking the interaction with downstream proteins, such as MAX2 proteins. This may indicate that our chemical library has great

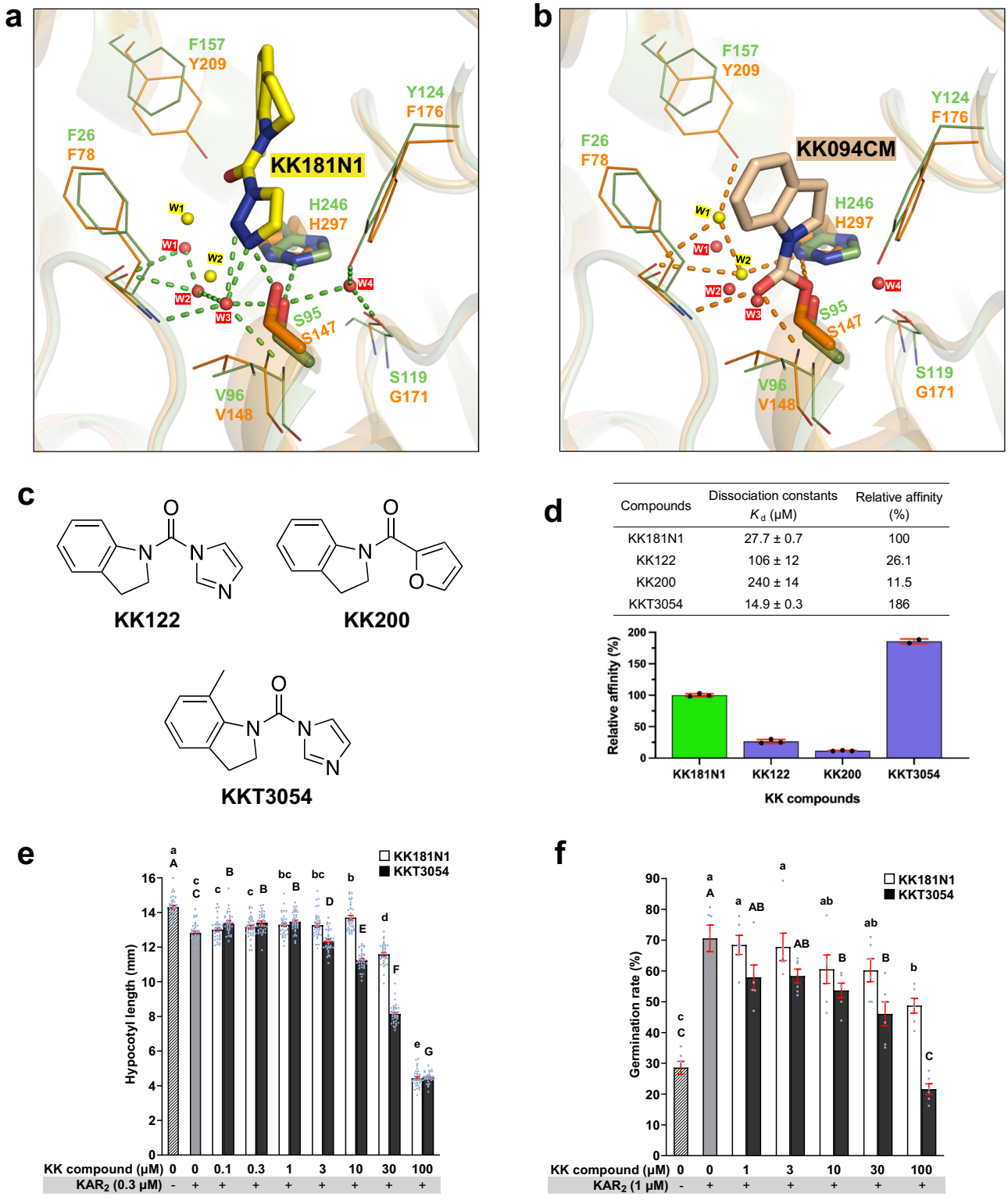

applicability for providing covalent and non-covalent probes for plant ABH.

KK181N1 showed highly selective inhibitory activity against KARs signaling without disturbing SLs signaling. Previous studies of parasitic KAI2/HTL homologous proteins have demonstrated that the pocket size may determine the ligand type and affinity[30,35,42,43], which may also affect competitive binding of KK181N1. The ITC data revealed that KK181N1's binding affinity to AtKAI2 and Os/AtD14s was nearly the same (Supplementary Fig. 10a,b). However, in vivo studies showed that KK181N1 did not suppress the GR24-dependent inhibition of the hypocotyl length in the *Arabidopsis kai2* mutant (Fig. 1f), nor did it cause the increased tiller number observed in rice due to the deletion of SL signaling (Supplementary Fig. 11a,c). These data suggest that KK181N1 binds to D14 but may not effectively inhibit the induction of SL-mediated signaling required for the expression of biological activity. We found that residue Y124, which prominently decreases the size of the ligand binding pocket by dividing it into two pockets, strongly stabilizes KK181N1 within the catalytic pocket by π-π interaction and

Fig. 4 | Triazole urea compounds participate in a water-mediated hydrogen bond network in AtKAI2 and OsD14. Comparison of the hydrogen-bonding networks in AtKAI2-KK181N1 (**a**, green) and OsD14-KK094CM (**b**, orange). KK181N1 and KK094CM are represented by yellow and wheat sticks, respectively. Four water molecules from AtKAI2-KK181N1 are labeled W1 to W4 in red shadow, and two from OsD14-KK094CM are labeled W1 and W2 in yellow shadow. Hydrogen bonds are indicated by green (**a**) or orange (**b**) dashed lines. **c** Chemical structures of KK122, KKT3054, and KK200. **d** The binding affinity of AtKAI2 to KK compounds, measured by ITC assays. The relative affinity is calculated with K_d values for comparison. Data are means of 2 or 3 technical replicates (mean ± SD). **e** Hypocotyl growth of wild-type *Arabidopsis* seedlings in response to 0.3 μM KAR_2 supplemented with different concentrations of KK181N1 (white column) and KKT3054 (black column). Hypocotyl length was recorded after cultivation under fluorescent white light (30 μmol m^{-2} s^{-1}) at 22 °C for 48 h followed by red LED light (35 μmol m^{-2} s^{-1}) at 22 °C for 4 days. Values and bars represent the means ± SE (n = 34 (0.3 μM KAR_2 + 100 μM KK181), 35 (0 μM KAR_2, 0.3 μM KAR_2, 0.3 μM KAR_2 + 10 μM KK181, 0.3 μM KAR_2 + 30 μM KK181, 0.3 μM KAR_2 + 0.1 μM KOKT3054, 0.3 μM KAR_2 + 10 μM KOKT3054, 0.3 μM KAR_2 + 100 μM KOKT3054), 36 (0.3 μM KAR_2 + 0.1 μM KK181, 0.3 μM KAR_2 + 1 μM KOKT3054, and 0.3 μM KAR_2 + 30 μM KOKT3054), 37 (0.3 μM KAR_2 + 0.3 μM KK181, 0.3 μM KAR_2 + 1 μM KK181, 0.3 μM KAR_2 + 3 μM KK181, and 0.3 μM KAR_2 + 0.3 μM KOKT3054), and 38 (0.3 μM KAR_2 + 3 μM KOKT3054)). *Letters indicate significant difference ($P < 0.05$), as determined by one-way ANOVA followed by two-tailed Tukey's HSD test for multiple-pair comparisons. **f** The germination rate of wild-type *Arabidopsis* seeds treated with different concentrations of KK181N1 (white column) and KKT3054 (black column) in the presence of 1 μM KAR_2 was recorded. The seeds were first incubated at 28 °C under continuous fluorescent white light (20 μmol m^{-2} s^{-1}) for 48 h and then at 22 °C for an additional 48 h. Data are the results of 6 biological replicates of around 30 seeds each. Values and bars represent the means ± SE. *Letter indicate significant difference ($P < 0.05$), as determined by one-way ANOVA followed by two-tailed Tukey's HSD test for multiple-pair comparisons. Source data are provided as a Source Data file.

forced water-mediated hydrogen bonds (Fig. 4a). This residue was substituted with smaller hydrophobic amino acids in the D14 clade and KAI2i/d subclade of KAI2 (Fig. 3f). The resulting enlarged pocket probably functions to allow perception with high sensitivity by SLs[35]. This would explain why KK181N1 cannot suppress GR24-induced germination in *S. hermonthica* (Fig. 3c). However, despite this, we believe that our chemical has potential applications. For example, while *Striga* does not respond to karrikins for germination, complementation assays in *Arabidopsis* have shown that ShKAI2i and PaKAI2c (*Phelipanche aegyptiaca*) can restore seed dormancy when treated with KAR_1[35]. Therefore, our karrikin signaling-specific inhibitor, KK181N1, could serve as a valuable chemical tool to explore the biological functions of receptors like KAI2c in *Striga* and potentially other parasitic weeds. On the other hand, Xu et al. have suggested that structural differences in the cap domain dominantly affect pocket size in AtKAI2 and thought to be determinants of KAR/GR24 selectivity. The residues constituting this cap domain include L142, Y157, A161, G190, I193, F194, L218, and A219[30], among which 4 residues (Y157, A161, L218, and A219) play essential roles in recognizing the methyl group of KK181N1 in AtKAI2 (Supplementary Fig. 6d). KK181N1 inhibited KAR_1-induced seed germination of lettuce, probably by inhibiting the function of LsKAI2a, because LsKAI2a contains identical key residues of AtKAI2 to interact with KK181N1, whereas LsKAI2b has two different residues, F and V, which correspond to the positions 124 and 161 of AtKAI2, respectively (Fig. 3f). Affinity assay and structural analysis showed that Y124F substitution is deleterious for KK181N1-binding affinity (Fig. 3b), and A161V seems to cause the steric hindrance with the methyl group of KK181N1 (Supplementary Fig. 6d). However, a recent study revealed that LsKAI2b mainly mediates the KAR_1 response in lettuce[44]. This is consistent with the results that KK181N1 significantly suppressed KAR_1-stimulated seed germination but still maintained a higher germination rate than in the absence of KAR_1 treatment.

Overall, our results indicate that the KARs-specific pocket architecture also contributes to the high sensitivity of KK181N1 for KAI2. We further detected four structured water molecules involved in forming a hydrogen-bonding network at the pocket bottom, and their arrangement seems to be optimized for the noncovalent binding with KK181N1. Interestingly, the water mediated hydrogen-bonding network was formed between the water molecules and the oxyanion hole that is required for the catalytic reaction of ABH (Figs. 3h, 4a,b, and Supplementary Fig. 9b), implying that this network should be very conservative. Indeed, we also found intact or partial water-bridged hydrogen-bonding networks resembling AtKAI2-KK181N1 in D14, KAI2, and many ShHTL proteins. This study revealed that our in-house chemical library using the scaffold of triazole ureas is tremendously favored by the water molecules-mediated hydrogen-bonding network buried inside of the pocket. Moreover, we designed a distinct compound by fine-tuning this network, which suggests that considerable attention to structured water molecules in chemical tool design can produce inhibitors with improved or altered selectivity properties.

However, these compounds did not fully restore the KAR_2-dependent change in hypocotyl length. Given the importance of KAI2 signaling in plant growth, it would be expected that inhibitor treatments would show more pronounced effects. Further chemical modification to obtain potent and selective inhibitors of AtKAI2 are required to establish chemically controlled approaches to dissect KAR functions and signaling.

Genetic approaches using mutants have revealed universal KAR signaling and physiological functions of KARs, as well as the existence of KAR roles specific to different plant species[9,13,27,45–47]. This approaches usually provides direct results. However, it is still difficult to generate mutants in many plant species with current technology, and studies using model plants may not focus on the role of KARs specific to a particular plant species. Since direct regulation by this compound is applicable to a wide range of plants, future experiments with KK181N1 may provide useful information on the physiological role of KARs. In addition, chemical genetic approaches based on the combination of compounds and plant phenotypes have contributed to the identification of factors involved in the biosynthesis and signaling of numerous plant hormones[48]. KAR_1 was a screening tool for identification of *max2* mutants[13]. We propose that KK181N1 can be used to screen for mutants of constitutively active KAI2 signaling. This compound could contribute to the discovery of novel signaling regulators and the elucidation of the regulatory mechanisms of known signaling regulators. We believe that its application to these approaches could facilitate our understanding of KAR biology.

Methods

Chemicals

GR24 was synthesized as previously described method[49] with some modification. Briefly, sodium hydride and methyl formate were added under an N_2 atmosphere to a solution of the tricyclic lactone compound in diethyl ether. The mixture was stirred at room temperature for 15 h, and the reaction was quenched with 1 M HCl. The solution was then extracted with ethyl acetate (EtOAc). The organic layer was washed with brine and H_2O, and dried over Na_2SO_4 and concentrated. The remaining yellow oil and white solid were dissolved in *N*-methyl-2-pyrrolidone. Potassium carbonate and a solution of 5-bromo-3-methyl-2(5*H*)-furanone were added to the solution. The reaction mixture was stirred at room temperature for 24 h. After quenching with 1 M HCl, it was extracted with EtOAc. The organic layer was washed with brine and H_2O, and dried over Na_2SO_4 and concentrated in vacuo. The residual yellow oil was contained four stereoisomers of GR24. It was separated into (±)-GR24 and its isomer (±)−2′-*epi*-GR24 by silica gel column chromatography with EtOAc and hexane. We used (±)-GR24 with the same relative stereochemistry as (±)-strigol. KAR_1 and KAR_2 were

purchased from Toronto Research Chemicals (ON, Canada) and OlChemIm (Olomouc, Czech Republic), respectively. The physicochemical properties and synthesis procedure of triazole ureas are described in the Supplementary Information.

Hypocotyl elongation assay

SL- and KAR-insensitive mutants and their wild-type Arabidopsis (*Arabidopsis thaliana*) were used. *atd14-1*, *atd14kai2*, and *max2-1* had a Columbia accession background, and *kai2-2* had a L*er* accession background. The seeds were sterilized with 70% (v/v) ethanol for 20 min and plated onto a 48-well plate (AGC Techno Glass, Shizuoka, Japan) containing half-strength Murashige and Skoog (MS) medium (pH=5.7) solidified with 0.8% agar and test compounds. The test compounds were diluted 1:1,000 from a dimethyl sulfoxide (DMSO)-dissolved stock solution (DMSO was used as the control). The plates were stratified in the dark at 4 °C for 48 h, exposed to fluorescent white light (30 μmol m^{-2} s^{-1}) for 48 h at 23 °C, and then incubated in continuous red LED light (35 μmol m^{-2} s^{-1}) for 4 days. The hypocotyls were scanned using a flatbed scanner, and the length of hypocotyls was measured using ImageJ software (https://imagej.nih.gov/ij/ [Date accessed: April 5, 2021]).

Seed germination assay

For seed germination assay using *Arabidopsis*, seeds (Columbia accession) were sterilized with 70% ethanol (v/v) for 20 min. The stratified seeds were sown onto a 96-well plate (AGC Techno Glass, Shizuoka, Japan) supplemented with 100 μL of 0.2% phytoagar containing the test compounds. The seeds were sown at a density of around 30 seeds per well. The plate was incubated at 30 °C under continuous fluorescent white light (20 μmol m^{-2} s^{-1}) for 48 h and then at 22 °C for an additional 36 h. The germination percentage was estimated by dividing the number of germinated seeds by the total number of seeds per well. For assessment of KOKT3054, the plate was incubated at 28 °C for 48 h followed by 22 °C for 48 h.

For the seed germination assay using lettuce (*Lactuca sativa*; Fringy green cultivar; Sakata Seeds, Japan), the sterilized seeds (around 50 seeds) were sown on filter paper disks saturated with 1 mL of distilled water containing the test compounds in a petri dish with a diameter of 60 mm (AGC Techno Glass). The test compounds were diluted at 1:1,000 from a DMSO-dissolved stock solution (DMSO was used as the control). The dishes were then covered with a double layer of aluminum foil, placed in an aluminum can to shield them from light, and incubated at 22 °C for 48 h. They were then examined for germination.

Molecular cloning and site-directed mutagenesis

The coding sequence of AtKAI2 was inserted into pET-48b(+) harboring an N-terminal Trx-His_6 tag at the *Bam*HI site. The reverse PCR-based site-directed mutagenesis was employed to prepare all the variants of AtKAI2 using a KOD-Plus-Mutagenesis Kit (TOYOBO). Mutagenesis was confirmed by systematic DNA sequencing. The primer sequences are shown in supplementary Table 3. Plasmid construction for the expression and purification of OsD14 and AtD14 is according to our previous studies[25,30].

Protein expression and purification

Protein expression and purification of AtKAI2, OsD14, and AtD14 were in the similar manner as described previously[11,25,30]. Using AtKAI2 as example described below. *Escherichia coli* Rosetta2 (DE3) (Novagen) was transformed with the recombinant vectors for protein expression. 20 mL of overnight seeding cultures was inoculated to 2 liters of fresh Luria-Bertani broth containing 25 μg/mL kanamycin at 37 °C until the OD_{600} reached 0.6–0.8. Protein expression was then induced by adding 0.1 mM isopropyl-β-D-thiogalactoside (IPTG) and incubating at 18 °C for 24 h. The cells were harvested and resuspended in buffer A (20 mM Tris–HCl (pH 8.0), 300 mM NaCl, 10 mM imidazole and 1 mM dithiothreitol (DTT)). After cell lysis with sonication, centrifugation (Avanti J-E rotor; Beckman Coulter) was performed at 40,000 × *g* and 4 °C for 30 min to remove cell debris. The supernatant fractions were collected and gently incubated with 2 mL of pre-equilibrated Ni-NTA Agarose (Qiagen) at 4 °C. 30 min later, the supernatant-resin mixtures were added to a disposable polypropylene column (Bio-Rad) and then washed by 50 mL of buffer A. The on-column removal of N-terminal Trx-His_6 tag was performed overnight at 4 °C by adding 40 μg HRV3C protease. Afterwards, a certain amount of buffer B (20 mM Tris–HCl (pH 8.0), 500 mM NaCl, 5% glycerol, 10 mM imidazole and 1 mM DTT) was used to elute untagged target proteins. AtKAI2 was further purified by employing anion exchange chromatography (Mono Q 10/100 GL; Cytiva) using a buffer consisting of 20 mM Tris–HCl (pH 8.0), 1 mM DTT, and a linear NaCl gradient from 0 to 1 M. The fraction was collected and examined by SDS-PAGE. Protein concentration was adjusted as needed by using a NanoDrop 2000 spectrophotometer (Thermo Scientific) at 280 nm absorbance.

Isothermal titration calorimetry

Isothermal titration calorimetry (ITC) experiments for the binding assays of AtKAI2, its variants, OsD14, and AtD14 with compounds were performed with a MicroCal iTC200 (Malvern). Prior to the measurements, the protein solution was dialyzed for 20 h against buffer C (20 mM HEPES (pH 8.0) and 150 mM NaCl) and adjusted to 150 μM. The remaining dialyzed buffer was used to prepare a ligand solution containing 1% DMSO at 2–5 mM. The sample cell and syringe were respectively filled with 204 μL of protein solution and 40 μL of ligand solution. For a given experiment, 19 consecutive 2.0-μL aliquots of ligand solution were injected into sample cells at 20 °C with a stirring speed of 750 rpm, reference power of 5 μcal s^{-1} and spacing of 150 s between injections. A negative control was made by titrating ligand solution into the dialyzed buffer containing 1% DMSO. For data analysis, all peaks, after excluding the first peak resulting from the initial 0.4 μL injection, were integrated corresponding to each injection, and the correction for the baseline and the fitting were performed using the Origin 7.0 software in the "one set of sites" mode, to obtain the dissociation constant (K_d). Three replicates were made for each measurement.

Crystallization, data collection and structure determination

The protein-ligand solution for co-crystallization trials was made by incubating 0.7 mg/mL of purified AtKAI2 solution with 5 mM KK181N1 at room temperature for 0.5–1 h, and then concentrated to 7 mg/mL using VivaSpin with a 10 kDa MWCO. Crystals of the AtKAI2–KK181N1 complex were generated by the sitting-drop vapor diffusion method at 20 °C from a 1:1 mixture of protein-ligand solution and reservoir solution (1.7 M sodium phosphate (pH 7.0) and 1% 1,2-butanediol).

A single crystal was picked up and soaked in reservoir solution containing 30% sucrose as a cryoprotectant, and then flash-cooled with a nitrogen-gas stream at 100 K. All X-ray diffraction data were collected using a wavelength of 1.080 Å on the BL-1A beamline at the Photon Factory (Tsukuba, Japan) and processed using the XDS package[50]. Molecular replacement was performed using Phaser in PHENIX[51] with the *apo*-KAI2 structure (PDB: 4JYP)[34] as the initial model. The model building and ligand fitting were performed by COOT[52] and further refined through iterative refinement cycles in PHENIX. Data collection and refinement statistics are presented in Supplementary Table 1. All structures were depicted by using PyMOL 2.5.4.

Protein sequence analysis and phylogenetic construction

A total of 424 KAI2/HTL and D14 sequences from angiosperms were identified from BLAST searches using Arabidopsis coding sequences AtKAI2 as a query. Parasitic KAI2/HTL genes were manually selected. Duplicate sequences were removed by manual inspection. Multiple sequence alignments were then performed using MAFFT (Multiple Alignment using Fast Fourier Transform). The alignment was trimmed slightly at the 5′-end to remove non-aligned and non-conserved regions of monocot D14 sequences. Maximum likelihood phylogeny

was constructed by Phylogeny.fr[53] based on the sequence alignment, and further displayed by an online tool, interactive tree of life (iTOL) v6. The graphic representations of amino acids conservation were created using the WebLogo (https://weblogo.threeplusone.com/).

Additionally, the KAI2/HTL and D14 sequences from *Oryza sativa* (Os), *Arabidopsis thaliana* (At), *Lactuca sativa* (Ls), *Striga hermonthica* (Sh), and *Petunia hybrida* (Ph, D14 ortholog DAD2) were aligned using CLUSTAL OMEGA with default parameters, and the results were displayed via ESPript 3.0.

Statistical analysis

The data were analyzed with one-way ANOVA followed by two-tailed Tukey's HSD test using GraphPad Prism 9 (GraphPad Software, CA, USA). Statistical significance was defined as $P < 0.01$ or $P < 0.05$.

Reporting summary

Further information on research design is available in the Nature Portfolio Reporting Summary linked to this article.

Data availability

The atomic coordinates and structure factors of AtKAI2-KK181N1 have been deposited in the Protein Data Bank (PDB) under accession code 8Y9O. Source data are provided with this paper as Source Data 1 and Source Data 2. Other data supporting the findings of this manuscript are available from the corresponding author upon request.

References

1. Pausas, J. G. & Keeley, J. E. Wildfires as an ecosystem service. *Front. Ecol. Environ.* **17**, 289–295 (2019).
2. Raison R. J., Khanna, P. K., Jacobsen, K. L., Romanya, J. & Serra-solses, I. Effects of fire on forest nutrient cycles. *Fire effects on soils and restoration strategies*, 225-256 (2009).
3. Roche, S., Dixon, K. W. & Pate, J. S. Seed ageing and smoke: Partner cues in the amelioration of seed dormancy in selected Australian native species. *Aust. J. Bot.* **45**, 783–815 (1997).
4. Flematti, G. R., Ghisalberti, E. L., Dixon, K. W. & Trengove, R. D. A compound from smoke that promotes seed germination. *Science* **305**, 977–977 (2004).
5. Flematti, G. R., Ghisalberti, E. L., Dixon, K. W. & Trengove, R. D. Identification of alkyl substituted 2H-Furo[2,3-c]pyran-2-ones as germination stimulants present in smoke. *J. Agr. Food Chem.* **57**, 9475–9480 (2009).
6. Flematti, G. R. et al. Structure-activity relationship of karrikin germination stimulants. *J. Agr. Food Chem.* **58**, 8612–8617 (2010).
7. Nelson, D. C. et al. Karrikins enhance light responses during germination and seedling development in *Arabidopsis thaliana*. *Proc. Natl Acad. Sci. USA* **107**, 7095–7100 (2010).
8. Waheed, M. A., Jamil, M., Khan, M. D., Shakir, S. K., & Rehman, Shafiq-Ur. Effect of plant-derived smoke solutions on physiological and biochemical attributes of maize (*Zea Mays* L.) under salt stress. *Pak. J. Bot.* **48**, 1763–1774 (2016).
9. Gutjahr, C. et al. Rice perception of symbiotic arbuscular mycorrhizal fungi requires the karrikin receptor complex. *Science* **350**, 1521–1524 (2015).
10. Umehara, M. et al. Structural requirements of strigolactones for shoot branching inhibition in *Rice* and *Arabidopsis*. *Plant Cell Physiol.* **56**, 1059–1072 (2015).
11. Yao, R. F. et al. DWARF14 is a non-canonical hormone receptor for strigolactone. *Nature* **536**, 469–473 (2016).
12. Sun, X. D. & Ni, M. HYPOSENSITIVE TO LIGHT, an Alpha/Beta fold protein, acts downstream of ELONGATED HYPOCOTYL 5 to regulate seedling de-etiolation. *Mol. Plant* **4**, 116–126 (2011).
13. Nelson, D. C. et al. F-box protein MAX2 has dual roles in karrikin and strigolactone signaling in *Arabidopsis thaliana*. *Proc. Natl Acad. Sci. USA* **108**, 8897–8902 (2011).
14. Soundappan, I. et al. SMAX1-LIKE/D53 family members enable distinct MAX2-dependent responses to strigolactones and karrikins in *Arabidopsis*. *Plant Cell* **27**, 3143–3159 (2015).
15. Stanga, J. P., Smith, S. M., Briggs, W. R. & Nelson, D. C. SUPPRESSOR OF MORE AXILLARY GROWTH2 1 controls seed germination and seedling development in *Arabidopsis*. *Plant Physiol.* **163**, 318–330 (2013).
16. Zhou, F. et al. D14-SCFD3-dependent degradation of D53 regulates strigolactone signaling. *Nature* **504**, 406–410 (2013).
17. Wang, L. et al. Strigolactone signaling in *Arabidopsis* regulates shoot development by targeting D53-Like SMXL repressor proteins for ubiquitination and degradation. *Plant Cell* **27**, 3128–3142 (2015).
18. Swarbreck, S. M., Guerringue, Y., Matthus, E., Jamieson, F. J. C. & Davies, J. M. Impairment in karrikin but not strigolactone sensing enhances root skewing in *Arabidopsis thaliana*. *Plant J.* **98**, 607–621 (2019).
19. Wang, L. et al. Strigolactone and karrikin signaling pathways elicit ubiquitination and proteolysis of SMXL2 to regulate hypocotyl elongation in *Arabidopsis*. *Plant Cell* **32**, 2251–2270 (2020).
20. Swarbreck, S. M., Mohammad-Sidik, A. & Davies, J. M. Common components of the strigolactone and karrikin signaling pathways suppress root branching in *Arabidopsis*. *Plant Physiol.* **184**, 18–22 (2020).
21. Scaffidi, A. et al. Strigolactone hormones and their stereoisomers signal through two related receptor proteins to induce different physiological responses in *Arabidopsis*. *Plant Physiol.* **165**, 1221–1232 (2014).
22. Conn, C. E. & Nelson, D. C. Evidence that KARRIKIN-INSENSITIVE2 (KAI2) receptors may perceive an unknown signal that is not karrikin or strigolactone. *Front Plant Sci.* **6**, 1219 (2016).
23. Jiang, K. & Asami, T. Chemical regulators of plant hormones and their applications in basic research and agriculture. *Biosci. Biotech. Bioch.* **82**, 1265–1300 (2018).
24. Holbrook-Smith, D., Toh, S., Tsuchiya, Y. & McCourt, P. Small-molecule antagonists of germination of the parasitic plant *Striga hermonthica*. *Nat. Chem. Biol.* **12**, 724–729 (2016).
25. Nakamura, H. et al. Triazole ureas covalently bind to strigolactone receptor and antagonize strigolactone responses. *Mol. Plant* **12**, 44–58 (2019).
26. Thussagunpanit, J. et al. Involvement of STH7 in light-adapted development in *Arabidopsis* thaliana promoted by both strigolactone and karrikin. *Biosci. Biotech. Bioch.* **81**, 292–301 (2017).
27. Waters, M. T. et al. Specialisation within the DWARF14 protein family confers distinct responses to karrikins and strigolactones in *Arabidopsis*. *Development* **139**, 1285–1295 (2012).
28. Fukui, K., Arai, K., Kasahara, H., Asami, T. & Hayashi, K. Synthetic agonist of HTL/KAI2 shows potent stimulating activity for *Arabidopsis* seed germination. *Bioorg. Med. Chem. Lett.* **29**, 2487–2492 (2019).
29. Stirnberg, P., van de Sande, K. & Leyser, H. M. O. MAX1 and MAX2 control shoot lateral branching in Arabidopsis. *Development* **129**, 1131–1141 (2002).
30. Xu, Y. Q. et al. Structural analysis of HTL and D14 proteins reveals the basis for ligand selectivity in Striga. *Nat. Commun.* **9**, 3947 (2018).
31. Lee, I. et al. A missense allele of KARRIKIN-INSENSITIVE2 impairs ligand-binding and downstream signaling in *Arabidopsis thaliana*. *J. Exp. Bot.* **69**, 3609–3623 (2018).
32. Shannon, D. A. & Weerapana, E. Covalent protein modification: the current landscape of residue-specific electrophiles. *Curr. Opin. Chem. Biol.* **24**, 18–26 (2015).
33. Nardini, M. & Dijkstra, B. W. Alpha/beta hydrolase fold enzymes: the family keeps growing. *Curr. Opin. Struct. Biol.* **9**, 732–737 (1999).

34. Guo, Y. X., Zheng, Z. Y., La Clair, J. J., Chory, J. & Noel, J. P. Smoke-derived karrikin perception by the alpha/beta-hydrolase KAI2 from *Arabidopsis*. *Proc. Natl Acad. Sci. USA* **110**, 8284–8289 (2013).
35. Conn, C. E. et al. Convergent evolution of strigolactone perception enabled host detection in parasitic plants. *Science* **349**, 540–543 (2015).
36. Toh, S. et al. Structure-function analysis identifies highly sensitive strigolactone receptors in *Striga*. *Science* **350**, 203–207 (2015).
37. Yao, J. R. et al. An allelic series at the KARRIKIN INSENSITIVE 2 locus of *Arabidopsis* thaliana decouples ligand hydrolysis and receptor degradation from downstream signalling. *Plant J.* **96**, 75–89 (2018).
38. Toh, S., Holbrook-Smith, D., Stokes, M. E., Tsuchiya, Y. & McCourt, P. Detection of parasitic plant suicide germination compounds using a high-throughput *Arabidopsis* HTL/KAI2 strigolactone perception system. *Chem. Biol.* **21**, 988–998 (2014).
39. McConnell, D. B. Biotin's lessons in drug design. *J. Med. Chem.* **64**, 16319–16327 (2021).
40. Agalave, S. G., Maujan, S. R. & Pore, V. S. Click chemistry: 1,2,3-triazoles as pharmacophores. *Chem.-Asian J.* **6**, 2696–2718 (2011).
41. Arellano-Saab, A. et al. Structural analysis of a hormone-bound Striga strigolactone receptor. *Nat. Plants* **9**, 883–888 (2023).
42. Burger, M. & Chory, J. In-silico analysis of the strigolactone ligand-receptor system. *Plant Direct* **4**, e00263 (2020).
43. Burger, M. et al. Structural Basis of karrikin and non-natural strigolactone perception in *Physcomitrella patens*. *Cell Rep.* **26**, 855–865 (2019).
44. Martinez, S. E. et al. A KARRIKIN INSENSITIVE2 paralog in lettuce mediates highly sensitive germination responses to karrikinolide. *Plant Physiol.* **190**, 1440–1456 (2022).
45. Kameoka, H. & Kyozuka, J. Downregulation of rice DWARF 14 LIKE suppress mesocotyl elongation via a strigolactone independent pathway in the dark. *J. Genet. Genomics* **42**, 119–124 (2015).
46. Carbonnel, S. et al. Lotus japonicus karrikin receptors display divergent ligand-binding specificities and organ-dependent redundancy. *PLoS Genet* **16**, e1009249 (2020).
47. Mizuno, Y. et al. Major components of the KARRIKIN INSENSITIVE2-dependent signaling pathway are conserved in the liverwort Marchantia polymorpha. *Plant Cell* **33**, 2395–2411 (2021).
48. Dejonghe, W. & Russinova, E. Plant chemical genetics: From phenotype-based screens to synthetic biology. *Plant Physiol.* **174**, 5–20 (2017).
49. Mangnus, E. M., Dommerholt, F. J., Dejong, R. L. P. & Zwanenburg, B. Improved synthesis of strigol analog GR24 and evaluation of the biological-activity of its diastereomers. *J. Agr. Food Chem.* **40**, 1230–1235 (1992).
50. Kabsch, W. Xds. *Acta Crystallogr. D. Biol. Crystallogr.* **66**, 125–132 (2010).
51. Adams, P. D. et al. PHENIX: a comprehensive Python-based system for macromolecular structure solution. *Acta Crystallogr. D. Biol. Crystallogr.* **66**, 213–221 (2010).
52. Emsley, P. & Cowtan, K. Coot: model-building tools for molecular graphics. *Acta Crystallogr. D. Biol. Crystallogr.* **60**, 2126–2132 (2004).
53. Dereeper, A. et al. Phylogeny.fr: robust phylogenetic analysis for the non-specialist. *Nucleic Acids Res.* **36**, W465–W469 (2008).

Acknowledgements

The authors thank Prof. Steven M. Smith and Dr. Mark T. Waters (University of Western Australia, Australia) for kindly providing the *Arabidopsis kai2-2* mutant seeds and Prof. Abdelgabbar Eltayeb Babiker (Environment and Natural Resources and Desertification Research Institute, Sudan) for kindly providing the *S. hermonthica* seeds. We also thank Dr. Yoshiki Ikeda (Kyoto University, Japan), who kindly provided the opportunity to use the ITC instrument for several binding assays. This work was supported in part by a grant from the Core Research for Evolutional Science and Technology (CREST) Program of the Japan Science and Technology Agency (JST) (to T.A.); a JSPS Grant-in-Aid for Scientific Research (grant number JP18H05266 to T.A.); a grant from the Platform Project for Supporting Drug Discovery and Life Science Research (Basis for Supporting Innovative Drug Discovery and Life Science Research (BINDS)) from AMED (grant number JP24ama121010 to T.M.); a PhD scholarship from China Scholarship Council (to J.W.); and by funds from the Fostering Advanced Human Resources to Lead Green Transformation (GX) project in Support for Pioneering Research Initiated by Next Generation of JST (SPRING) (to J.W.). The synchrotron-radiation experiments were performed on the BL-1A beamline at the Photon Factory under the approval of the Photon Factory Program Advisory Committee (Proposal No. 2018G559).

Author contributions

T.M., M.T. and T.A. conceived the study. J.W., I.T., T.M., and Z.Z. performed the biochemical experiments with the support of T.N. J.W. performed sequence analysis. X-ray diffraction data was collected by J.W., Z.Z. and T.M. I.T. and T.S. performed the plant experiments under the guidance of J.K. K.K. synthesized chemicals. J.W., I.T., H.N., T.N., T.M., and T.A analyzed the data. J.W. and I.T. assembled the manuscript and wrote the paper with input from all authors. I.T. T.M. and T.A. revised the manuscript.

Competing interests

The authors declare no competing interests.

Additional information

Supplementary information The online version contains supplementary material available at https://doi.org/10.1038/s41467-024-54801-1.

Correspondence and requests for materials should be addressed to Takuya Miyakawa or Tadao Asami.

Peer review information *Nature Communications* thanks Yuichiro Tsuchiya, and the other, anonymous, reviewer(s) for their contribution to the peer review of this work. A peer review file is available.